LAWRENCE
LIVERMORE
NATIONAL
LABORATORY

UCRL-TR-213076

Evaluation of the Mathieu Function Series for Diffraction by a Slot

Gerald J. Burke, Hsueh-Yuan Pao

June 21, 2005

This work was performed under the auspices of the U.S. Department of Energy by University of California, Lawrence Livermore National Laboratory under Contract W-7405-Eng-48.

Evaluation of the Mathieu Function Series for Diffraction by a Slot *

G. J. Burke, H. Y. Pao
Lawrence Livermore National Laboratory, Livermore, CA 94550

Introduction

Diffraction of a wave passing through a slot is a fundamental problem that has applications in many situations. A problem of current interest is the propagation of waves through obstacles such as buildings in an urban environment, where an entrance aperture could be approximated as a slot. Solutions for the diffracted fields of a slot have been obtained by exact eigenfunction expansions as well as various approximate and numerical methods. The eigenfunction solution, in terms of Mathieu functions, has been published by Stamnes and Eide [1] for a slot with several types of converging incident waves. Results of the eigenfunction solution are presented in [2] for slots up to 20 wavelengths in width and compared with Kirchhoff and Debye approximations.

We have attempted to duplicate the eigenfunction series results in [2]. Little information is given in [2] about the numerical issues in the evaluation. We encountered a number of problems in the evaluation of the Mathieu functions for wide slots that required modifications of the Mathieu function evaluation methods described in [3]. Results were obtained matching those for the largest slot of 20λ in [2] and also for slots up to 40λ width. The evaluation of the eigenfunction solution was checked against a 2D moment method solution and was in close agreement up to a slot width of 40λ.

The eigenfunction solution published by Stamnes and Eide is summarized below, followed by a discussion of the Mathieu function evaluation and problems encountered with large slot widths. Results are then presented for varying slot width and compared with the 2D moment method solutions. A moment method solution for a diverging wave incident on the gap between two square cylinders is also presented and compared with the fields in a slot representing the front aperture.

Eigenfunction solution for diffraction by a slot

The solution for diffraction by a slot can be obtained by the separation of variables solution of the wave equation in elliptical coordinates. Results are presented by Stamnes in [1] for hard or soft screens and for an incident plane wave, converging cylindrical wave and converging dipole wave. The result for a hard screen, where the potential $u^{h,q}$ represents the magnetic field parallel to the slot, will be considered here and is

$$u^{h,q} = \sum_{m=0}^{\infty} Be_m(s) Ce_m^q(s) He_m^{(1)}(s,u) Se_m(s,v) \tag{1}$$

where u and v are the radial and angular elliptical coordinates, $s = (kD/2)^2$ for slot width D and $q = c$ for a converging cylindrical wave or $q = d$ for a converging dipole wave. The

* This work was performed under the auspices of the U. S. Department of Energy by the University of California, Lawrence Livermore National Laboratory under Contract No. W-7405-Eng-48.

coefficients Be are

$$Be_m(s) = (8\pi)^{1/2} \frac{i^m}{Ne_m} \frac{Je_m(s,0)}{He_m^{(1)}(s,0)}.$$

The functions $Se_m(s,v)$ are the angular Mathieu functions even in v, while $Je_m(s,u)$ are the radial Mathieu functions analogous to the J Bessel functions and $He_m^{(1)}(s,u)$ are radial Mathieu functions corresponding to the cylindrical Hankel functions $H_m^{(1)}$. These functions are discussed in the next section and evaluation methods are given in [3].

The functions $Ce_m^q(s)$ are called the integrated Mathieu functions by Stamnes, and depend on the incident wave. For a converging incident wave focused at a distance z_1 behind the screen they are defined as

$$Ce_{2r+\gamma}^q(s) = \sum_{k=0}^{\infty} De_{2k+\gamma}^{(2r+\gamma)}(s) Le_{2k+\gamma}^q(kz_1)$$

for $\gamma = 0, 1$. De_k^r are coefficients in the series solution of Mathieu's equation and are discussed in the next section and

$$Le_n^q(w) = \tfrac{1}{2}\left[L_n^{q+}(w) + L_n^{q-}(w)\right]$$

$$L_n^{d\pm}(w) = \frac{k}{2\pi} \int_0^{\pi} \sin t \exp[-i(w \sin t \mp nt]\, dt$$

$$L_n^{c\pm}(w) = \frac{k}{2\pi} \int_0^{\pi} \exp[-i(w \sin t \mp nt]\, dt.$$

The integrands for $L_n^{d\pm}$ and $L_n^{c\pm}$ show rapid oscillation when w is large. A method for evaluating these integrals is described in [6], where the integration range is divided into subdomains where the integrand is approximated by functions that can be integrated in terms of known functions. Rather than use this method we integrated numerically in the complex plane. For $n \le w$ the integrand for $L_n^{d\pm}$ has a saddle point on the real axis at $t_s = \cos^{-1}(\pm n/w)$ with the path of steepest descent and minimum phase change passing through at an angle $\pi/4$ in the complex plane. It can be integrated relatively easily by integrating from $t = 0$ to $-it_s$, then to $t = \pi + i(\pi - t_s)$ and then to π. The integrals away from the real axis can be terminated if the integrand decays to a sufficiently small value. The NIntegrate function was used in Mathematica and an adaptive Romberg quadrature routine in Fortran.

The coefficients Ne_m are defined as

$$Ne_{2r} = 2\pi(De_0^{2r})^2 + \pi \sum_{k=1}^{\infty} (De_{2k}^{2r})^2 = \int_0^{2\pi} [Se_{2r}(s,v)]^2\, dv \tag{2a}$$

$$Ne_{2r+1} = \pi \sum_{k=0}^{\infty} (De_{2k+1}^{(2r+1)})^2 = \int_0^{2\pi} [Se_{2r+1}(s,v)]^2\, dv. \tag{2b}$$

The elliptical coordinates u and v, radial and angular respectively, are related to rectangular coordinates as

$$x = a \cosh u \, \cos v \qquad z = a \sinh u \, \sin v$$

where a is the half-width of the slot. Solving for u and v yields

$$v = \cos^{-1}\left[\frac{x\sqrt{2}}{\left(a^2 + x^2 + y^2 + \sqrt{4(ay)^2 + (x^2 + y^2 - a^2)^2}\right)^{1/2}}\right]$$

$$u = \cosh^{-1}\left[\frac{1}{a\sqrt{2}}\left(a^2 + x^2 + y^2 + \sqrt{4(ay)^2 + (x^2 + y^2 - a^2)^2}\right)^{1/2}\right].$$

Evaluation of the Mathieu Functions

The Mathieu functions needed in the solution for diffraction by a slot are less commonly available than other functions such as Bessel functions. Methods of evaluation and tabulated values have been published by G. Blanch and others [4, 5]. Mathieu functions are solutions of the Mathieu differential equations

$$\frac{d^2 f(v)}{dv^2} - (c - \tfrac{1}{2}s\cos 2v) f(v) = 0 \tag{3a}$$

$$\frac{d^2 g(u)}{du^2} - (c - \tfrac{1}{2}s\cosh 2u) g(u) = 0 \tag{3b}$$

where u and v are the radial and angular elliptical coordinates and c and s are separation constants in the solution of the wave equation. Certain "characteristic values" of c make the solution periodic in v as required. The characteristic values can be evaluated from continued fraction expansions and coefficients in the series solutions for $f(v)$ are related by recursion relations [4]. Stamnes [3] has demonstrated a more direct procedure for these evaluations by writing the recursion relations in matrix form. The characteristic values are then eigenvalues of the matrices and the series coefficients are the eigenvectors.

It is convenient to separate the solutions into those even and odd in v and also separate those into solutions periodic in π or 2π. The basic angular solutions for Eq. 3a are then

$$Se_{2r}(s, v) = \sum_{k=0}^{\infty} De_{2k}^{(2r)}(s) \cos 2kv \tag{4a}$$

$$Se_{2r+1}(s, v) = \sum_{k=0}^{\infty} De_{2k+1}^{(2r+1)}(s) \cos(2k+1)v \tag{4b}$$

$$So_{2r}(s, v) = \sum_{k=1}^{\infty} Do_{2k}^{(2r)}(s) \sin 2kv \tag{4c}$$

$$So_{2r+1}(s, v) = \sum_{k=0}^{\infty} Do_{2k+1}^{(2r+1)}(s) \sin(2k+1)v \tag{4d}$$

where the coefficients De_k^r and Do_k^r for even and odd functions, respectively, are associated with the characteristic value number r. They are obtained from the recursion relations or as eigenvectors of the corresponding matrices. In Stamnes' papers [1] the coefficients are

normalized so that the even functions have unit value at $v = 0$ and the odd functions have derivatives of unity at $v = 0$. The normalized coefficients must then satisfy

$$\sum_{k=0}^{\infty} De_{2k}^{(r)} = \sum_{k=0}^{\infty} De_{2k+1}^{(r)} = 1 \tag{5a}$$

$$\sum_{k=1}^{\infty} 2k Do_{2k}^{(r)} = \sum_{k=0}^{\infty} (2k+1) Do_{2k+1}^{(r)} = 1. \tag{5b}$$

The radial solutions for Eq. 3b can be obtained by making the substitution $v \to iu$ in Eq. 4. However, the series would diverge except for small values of u. Alternate forms for the radial solutions have been obtained as sums of Bessel functions J_n. The radial Mathieu function analogous to the J Bessel functions can be evaluated as

$$Je_{2r+\gamma}(s,u) = (-1)^r \left(\frac{\pi}{2}\right)^{1/2} \sum_{k=0}^{\infty} (-1)^k De_{2k+\gamma}^{(2r+\gamma)} J_{2k+\gamma}(\sqrt{s}\cosh u) \tag{6a}$$

$$Jo_{2r+\gamma}(s,u) = (-1)^r \left(\frac{\pi}{2}\right)^{1/2} \tanh u \sum_{k=0}^{\infty} (-1)^k (2k+\gamma) Do_{2k+\gamma}^{(2r+\gamma)} J_{2k+\gamma}(\sqrt{s}\cosh u). \tag{6b}$$

for $\gamma = 0$, 1. An alternate form for the same solutions can be evaluated as sums of products of Bessel functions as

$$Je_{2r}(s,u) = (-1)^r \left(\frac{\pi}{2}\right)^{1/2} \frac{1}{De_0} \sum_{k=0}^{\infty} (-1)^k De_{2k}^{(2r)} J_k(\alpha) J_k(\beta) \tag{7a}$$

$$\begin{aligned} Je_{2r+1}(s,u) =& (-1)^r \left(\frac{\pi}{2}\right)^{1/2} \frac{1}{De_1} \sum_{k=0}^{\infty} (-1)^k De_{2k+1}^{(2r+1)} \\ & \times [J_{k+1}(\alpha) J_k(\beta) + J_k(\alpha) J_{k+1}(\beta)] \end{aligned} \tag{7b}$$

$$\begin{aligned} Jo_{2r}(s,u) =& (-1)^r \left(\frac{\pi}{2}\right)^{1/2} \frac{1}{Do_2} \sum_{k=1}^{\infty} (-1)^k Do_{2k}^{(2r)} \\ & \times [J_{k+1}(\alpha) J_{k-1}(\beta) - J_{k-1}(\alpha) J_{k+1}(\beta)] \end{aligned} \tag{7c}$$

$$\begin{aligned} Jo_{2r+1}(s,u) =& (-1)^r \left(\frac{\pi}{2}\right)^{1/2} \frac{1}{Do_1} \sum_{k=0}^{\infty} (-1)^k Do_{2k+1}^{(2r+1)} \\ & \times [J_{k+1}(\alpha) J_k(\beta) - J_k(\alpha) J_{k+1}(\beta)] \end{aligned} \tag{7d}$$

where

$$\alpha = \tfrac{1}{2}\sqrt{s}\exp(u), \qquad \beta = \tfrac{1}{2}\sqrt{s}\exp(-u).$$

An independent set of radial solutions, analogous to the cylindrical Neumann functions Y_n, can be obtained by replacing the Bessel functions $J_k(\alpha)$ by $Y_k(\alpha)$ in Eq. 7 to obtain

$$Ne_{2r}(s,u) = (-1)^r \left(\frac{\pi}{2}\right)^{1/2} \frac{1}{De_0} \sum_{k=0}^{\infty} (-1)^k De_{2k}^{(2r)} Y_k(\alpha) J_k(\beta) \tag{8a}$$

$$Ne_{2r+1}(s,u) = (-1)^r \left(\frac{\pi}{2}\right)^{1/2} \frac{1}{De_1} \sum_{k=0}^{\infty} (-1)^k De_{2k+1}^{(2r+1)} \times [Y_{k+1}(\alpha)J_k(\beta) + Y_k(\alpha)J_{k+1}(\beta)] \quad (8b)$$

$$No_{2r}(s,u) = (-1)^r \left(\frac{\pi}{2}\right)^{1/2} \frac{1}{Do_2} \sum_{k=1}^{\infty} (-1)^k Do_{2k}^{(2r)} \times [Y_{k+1}(\alpha)J_{k-1}(\beta) - Y_{k-1}(\alpha)J_{k+1}(\beta)] \quad (8c)$$

$$No_{2r+1}(s,u) = (-1)^r \left(\frac{\pi}{2}\right)^{1/2} \frac{1}{Do_1} \sum_{k=0}^{\infty} (-1)^k Do_{2k+1}^{(2r+1)} \times [Y_{k+1}(\alpha)J_k(\beta) - Y_k(\alpha)J_{k+1}(\beta)]\,. \quad (8d)$$

Replacing J by Y in Eq. 6 yields a solution to Eq. 3b, but it is not the same as Eq. 8. Radial Mathieu functions analogous to the cylindrical Hankel functions are defined as

$$He_r^{(1)}(s,u) = Je_r(s,u) + iNe_r(s,u)$$
$$He_r^{(2)}(s,u) = Je_r(s,u) - iNe_r(s,u).$$

For the slot diffraction problem, the parameter s is related to the slot width D as $s = (ka)^2$ where $a = D/2$. For large slots s can be very large, causing problems in the function evaluations. Published tables of Mathieu functions, as in [4, 5], typically include s up to 100, while for a slot width of 20λ, $s = 3948$. With increasing s the coefficients $De_k^{(r)}$ and $Do_k^{(r)}$ oscillate positive and negative with increasing cancellation for $k > r$, so the normalization required in Eq. 5 can become difficult or impossible to obtain. When the normalization of Eq. 5 is possible the largest values of the normalized coefficients for $r = 0$ increase approximately as

$$\max |De_k^{(0)}| \approx \exp(-1.4 + 0.96\sqrt{s}). \quad (9)$$

For $s = 1400$ the maximum normalized coefficients are on the order of 10^{15}, so summing to 1.0 is at or beyond the limits of double precision arithmetic. Coefficients $De_{2k}^{(2r)}$ for $s = 4000$ normalized to sum to unity at the default precision of Mathematica are plotted in Fig. 1 for several values of r. The De_{2k}^{0} coefficients have a peak value of $1.5(10^{15})$, while Eq. 9 would predict a peak for the correctly normalized coefficients of around 10^{25}. For $s = 4000$ normalization appears to become possible for approximately $r = 10$ and above.

Other normalizations are sometimes applied to the functions, such as making Ne_{2r} and Ne_{2r+1} in Eq. 2 equal to $1/\pi$, which is used in [5]. However, this may shift the problems to other stages of the evaluation. It is noted in [4], which uses the normalization of Eq. 5, that coefficients had been obtained for $s = 6400$ but the result yields merely 0 for $v \leq 55°$, and it is stated ([4] page xxviii) that if another normalization were used which could be determined more easily, the results would still be unsatisfactory. However, while it may be unsatisfying mathematically that the function cannot be evaluated over its entire domain, the result may still be usable for the slot diffraction problem. When the values are significant the terms add constructively, and normalization errors may be reduced in some cases by cancellation in Eq. 1.

Asymptotic approximations for the angular functions $Se_r(s,v)$ for large s are given in [4], but they fail near $v = \pi/2$. An alternative Taylor series is given in [4] for v near $\pi/2$. However, piecing these approximations together over the range of parameters needed for the slot does not look promising. A comparison of the series and asymptotic evaluations for $s = 1000$ with $r = 2$ and 6 is shown in Fig. 2. The region of failure for the asymptotic form expands rapidly about $\pi/2$ with increasing r. The asymptotic form does go accurately to 1.0 at $v = 0$ though, so it might be useful for getting an accurate normalization of the series coefficients by matching values. From a comparison of the series and asymptotic forms for Se it appears that the function can be evaluated accurately from the series for large values of s except for the failure of the normalization for s larger than about 1400.

The evaluation of the radial functions also runs into problems with large s when the series in Eq. 1 must be summed to a higher number of terms for convergence. The coefficients De_k^r decay rapidly for k much less or greater than r, as seen in Fig. 1. With both the Mathematica and double precision LAPACK eigenvector routines the coefficients underflowed to zero when they became less than about 10^{-22} of the peak value in the eigenvector. This underflow prevents the use of Eq. 7 series, since the terms are normalized by the first coefficient which could become zero. It was found that accurate values of these small coefficients can be obtained by using forward and backward recursion in the direction of increasing values. The lower and upper sections of the vector De_k^r from recursion for each value of r were then normalized to match at $k = r$ and they were then normalized as well as possible over all k to satisfy Eq. 5. Thus the characteristic values were obtained from the eigenvalue solution, but the coefficients were obtained by recursion.

Another problem was in the choice of using Eq. 6 or 7 for Je. Some references state that the product form of Eq. 7 converges faster than 6, although it involves more Bessel function evaluations. Stamnes [3] suggests using Eq. 6 when $u > 5 - 0.043s$ and Eq. 7 otherwise. However, it was found that the sums in Eq. 7 could not converge for larger values of r. A typical result is shown in Fig. 3, where the summation of Eq. 7 for $Je_{2r}(s,u)$ diverges for r greater than 15 with $s = 400$. The asymptotic approximation of $Je_{2r}(s,u)$ for large s from [4] is also shown in Fig. 3 and is seen to fail as soon as the function starts to decay with increasing r. This limitation of the asymptotic approximation was also seen with s as large as 4000.

The reason for the divergence of Eq. 7 can be seen in Fig. 4, where the partial sums in Eq. 6a and 7a from 0 to n are plotted versus n. Note that the coefficients $De_{2k}^{(2r)}$ in Eq. 7a are renormalized by the first coefficient $De_0^{(2r)}$. As can be seen in Fig. 1, for larger values of r the $De_0^{(2r)}$ coefficient may be much smaller than the unity normalization established by Eq. 5. The Bessel function terms in both equations are of a similar order of magnitude and decay with increasing order for fixed argument. Hence the terms in Eq. 7 may start out much larger and have to converge to the same value as Eq. 6. In Fig. 4 it is seen that the convergence for $Je_{2r}(s,u)$ is successful for $r = 1$ and 8. For $r = 10$, Eq. 7 fails to converge by about a factor of 14, while for $r = 25$ it has the hopeless task of converging over 50 orders of magnitude. The odd ordered functions behave in a similar way.

Combining even and odd orders, the summations in Eq. 7 for $Je_r(s,u)$ were found to fail for r larger than about $13 + 0.7\sqrt{s}$ for $u = 0$ and for $r > 15 + 1.1\sqrt{s}$ for $u = 0.88$. The sum

in Eq. 6 was also found to fail for $r < 18$ with $s = 4000$. Hence we used $Je_r(s,u)$ from Eq. 6 for $r > 6 + 0.7\sqrt{s}$ and Eq. 7 for smaller r. Generalized forms of Eq. 7 with normalization to any coefficient De_s^r are given in [5] and may also offer a solution to this problem.

With the use of recursion rather than the eigenvectors and appropriate choice of Eq. 6 or 7 it appears that the Mathieu functions can be evaluated accurately except for the failure of normalization for s greater than about 1400. So how does the normalization error effect the evaluation of Eq. 1? The terms in the summation in Eq. 1 fall off slowly for m up to about $0.6\sqrt{s}$ and then decrease exponentially. This break point is just before the switch from Eq. 7 to Eq. 6 for Je. Hence most of the contribution to the sum comes from terms with $Je_r(s,u)$ from Eq. 7 with the normalization error canceled by the division by the first coefficient. The $Ne_r(s,u)$ functions are also free of the normalization error. The normalization error then shows up squared in Ne_m in the denominator of $Be_m(s)$ and in $Ce_m^q(s)$ and $Se_m(s,v)$ in Eq. 1, so it should cancel out.

Results for Diffraction by a Slot

Stamnes in [2] presents results for diffraction of a converging dipole wave focused behind slots of varying width. The geometry of the problem is shown in Fig. 5, where the wave is focused at z_1 with incident field normalized to 1.0 at the center of the slot. The dipole wave is the derivative with respect to z of a converging cylindrical wave. We have attempted to reproduce these results using Stamnes' solution with modifications to the evaluation as described in the previous section.

The results of the Mathieu function solution were compared with a 2D moment method solution. The moment method code was written for a strip with E parallel to the infinite strip axis, so that only current parallel to the slot and the resulting vector potential needs to be considered. After application of Babinets principle, this solution yields the result for H parallel to the slot. So, while Stamnes presented results for both E and H parallel to the slot, only the H_y polarization is considered here. The slot width was divided into about 50 sections per wavelength for the moment method solution, although fewer sections by at least a factor of two probably would give accurate results.

Results for a slot width D of 5λ with focus at $z_1 = 2.5\lambda$ are shown in Fig. 6 and 7. The contour and density plots in Fig. 6 were produced with the 2D moment method code, since that code written in Fortran was much faster than the Mathieu function evaluation in Mathematica. The contour plot appears to match that of Fig. 11b in [2]. Plots of H_y along the z axis and versus x at several z values are shown in Fig. 7. The Mathieu function and moment method solutions are seen to be in close agreement and match the plots in Fig. 11c through h in [2]. The Mathieu function evaluation used coefficient matrices of order 32, so the total number of characteristic values for $2r$ and $2r + 1$ values was 64. Results in Fig. 8 and 9 for a slot width of 10λ with the focus at $z_1 = 10\lambda$ also show close agreement between the Mathieu function solution and moment method and match the plots in Fig. 7 in [2]. A similar set of plots are shown in Fig. 10 and 11 for a slot width of 20λ and focus at $z_1 = 10\lambda$. For this slot width the Mathieu function evaluation summing over 64 characteristic values diverged for small values of z and was also inaccurate for x out of the main beam. Summing 128 characteristic values gave accurate agreement with the moment method and with Stamnes' plots in Fig. 3 of [2]. Results for a slot width of 40λ and $z_1 = 20\lambda$ are shown in Fig. 12 and 13 with good agreement between Mathieu function and moment method results.

Summing 128 terms was not accurate for the 40λ width, so we used 256 terms.

To model the propagation of a wave between obstacles such as buildings the Mathieu function solution for diffraction by a slot could be used to approximate the field in an entrance aperture and then be coupled with a waveguide model for propagation between the obstacles. The moment method code can provide a check on this approach by modeling the buildings as 2D cylinders as long as the dimensions are not too large. The moment method solution for propagation between two 10λ square cylinders with a 5λ gap is shown in Fig. 14a and is compared with result for only the front walls forming a slot. The surfaces were divided into about 20 strips per wavelength for the solution. The source in this case is a line current in front of the cylinders at $z = -5\lambda$ and the electric field E_y is shown since Babinet's principle was not applied. The slot in Fig. 14b was formed between two 10λ wide conducting screens. Some error fields can be seen inside the 10λ cylinders, since they make good resonators. The fields in the front aperture between the cylinders and in the slot are compared in Fig. 15 and are seen to be close enough so that the slot solution could probably be used to approximate the excitation of waveguide modes between the buildings.

Conclusion

The diffraction of a wave passing through a slot has been evaluated from the exact solution in terms of Mathieu functions published by Stamnes [1]. The results agree well with published results in [2] and are in close agreement with a 2D moment method solution. The difficulty in evaluating the Mathieu function solution for large slots is in accurately evaluating the Mathieu functions for large values of the parameter s. We used the eigenvalue method published by Stamnes to get the characteristic values, but to avoid premature underflow we used forward and backward recursion rather than the eigenvectors to get the series coefficients for the Mathieu functions. A problem in the Mathieu function evaluation was the normalization for unit value of the angular functions at zero argument. Alternate normalizations, such as the sum of the squares of the coefficients, might avoid this problem, but also might shift it to another stage of the evaluation. The normalization error was found to nearly cancel out with an appropriate choice of the radial function evaluation.

The Mathieu function solution was evaluated for slot widths up to 40λ with good agreement with a 2D moment method solution. It was found that for accuracy sufficient to avoid a perceptible difference of curves on a plot the number of Mathieu functions summed (characteristic values) should be at least four times the slot width in wavelengths. We were unable to get accurate results for a slot width of 60λ.

Evaluation of the Mathieu function solution was fairly slow in Mathematica, taking about 20 seconds for each field evaluation with 128 characteristic values. Most of this time is spent in evaluating Bessel functions for the series evaluation of the radial Mathieu functions. Mathematica's built in Bessel function routines were used, which are evaluated for each order and argument, and the same Bessel functions were evaluated repeatedly for each order of the Mathieu functions. The efficiency of the code could be greatly improved by using recursion to get the Bessel functions for all needed orders in one evaluation and by saving the values for each different Mathieu function order. At the end of this work a Fortran code was completed using recursion for the Bessel functions and it takes about 0.004 seconds for a field evaluation with 128 characteristic values of the Mathieu functions.

References

[1] J. J. Stamnes and H. A. Eide, "Exact and approximate solutions for focusing of two-dimensional waves. I. Theory," *J. Opt. Soc. Am. A*, Vol. 15, No. 5, pp. 1285-1291, 1998.

[2] H. A. Eide and J. J. Stamnes, "Exact and approximate solutions for focusing of two-dimensional waves. II. Numerical comparisons among exact, Debye, and Kirchhoff theories," *J. Opt. Soc. Am. A*, Vol. 15, No. 5, pp. 1292-1307, 1998.

[3] J. J. Stamnes and B. Spjelkavik, "New method for computing eigenfunctions (Mathieu functions) for scattering by elliptical cylinders," *Pure Appl. Opt.*, Vol. 4, pp. 251-262, 1995.

[4] Staff of the Computation Lab., *Tables Relating to Mathieu Functions*, 2nd Ed., National Bureau of Standards, Applied Mathematics Series 59, U. S. Government Printing Office, Washington D.C, 1967.

[5] M. Abramowitz and I. A. Stegun, Eds., *Handbook of Mathematical Functions*, Ch. 20 by G. Blanch, "Mathieu Functions," NBS Applied Mathematics Series 55, U. S. Government Printing Office, Washington D.C, 1972.

[6] J. J. Stamnes, B. Spjelkavik and H. M. Pedersen, "Evaluation of diffraction integrals using local phase and amplitude approximations," *Opt. Acta*, Vol. 30, pp. 207-222, 1983.

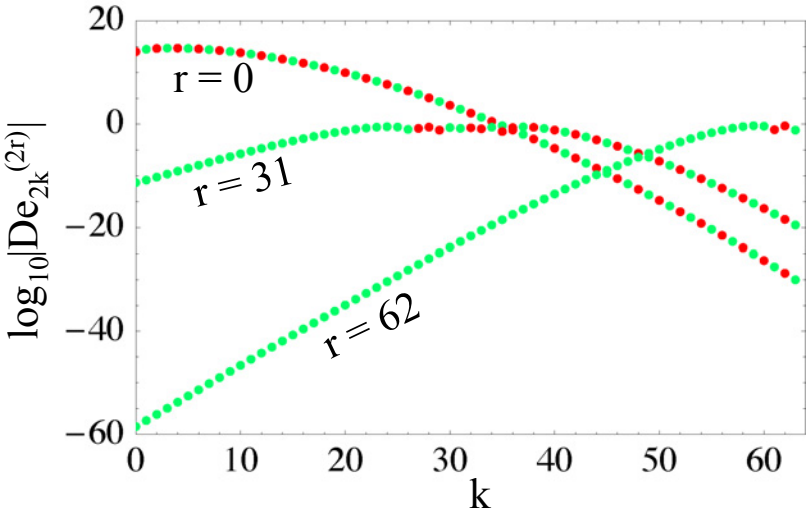

Fig. 1. Coefficients $De_{2k}^{(2r)}$ for $s = 4000$. Green points represent positive values and red points are negative.

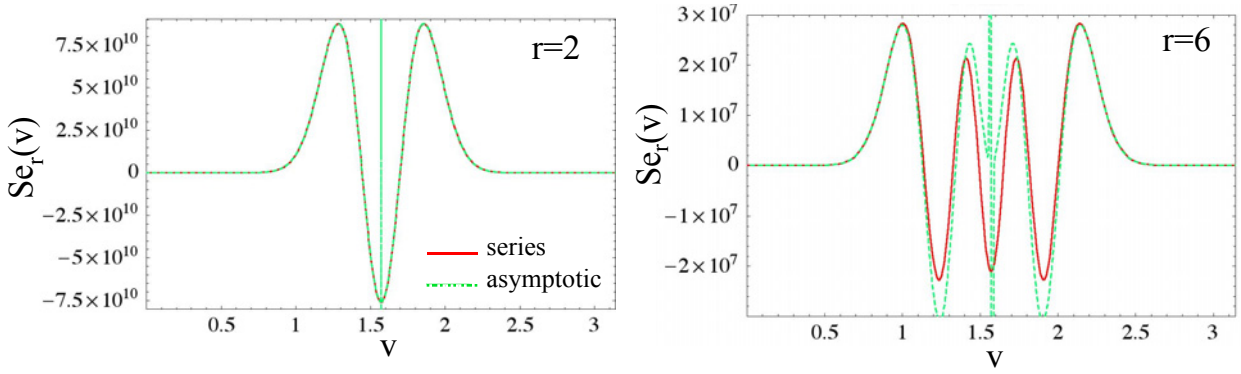

Fig. 2. Angular Mathieu function $Se_r(s, v)$ from series and asymptotic forms for $r = 2$ and 6 with $s = 1000$. The asymptotic approximation fails near $v = \pi/2$ over a region that expands with increasing r.

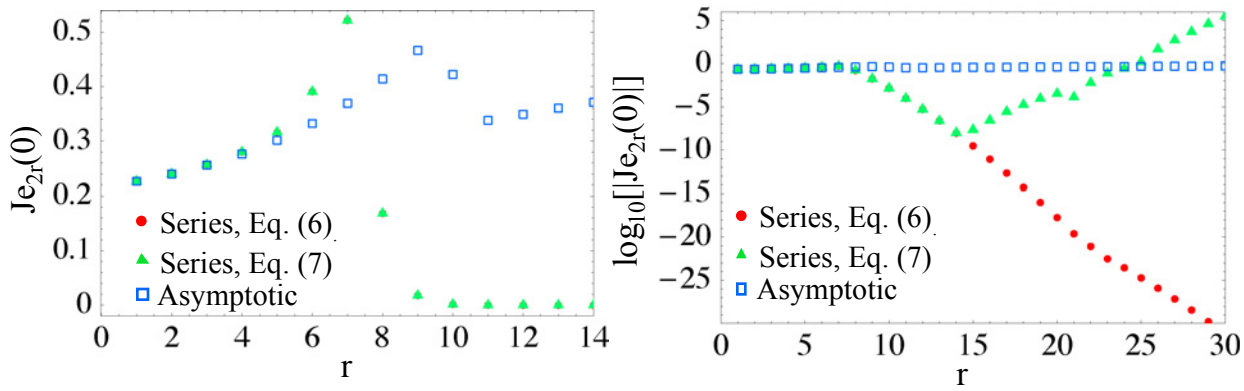

Fig. 3. Radial Mathieu functions $Je_{2r}(s, u)$ for $s = 400$ comparing series and asymptotic form for large s.

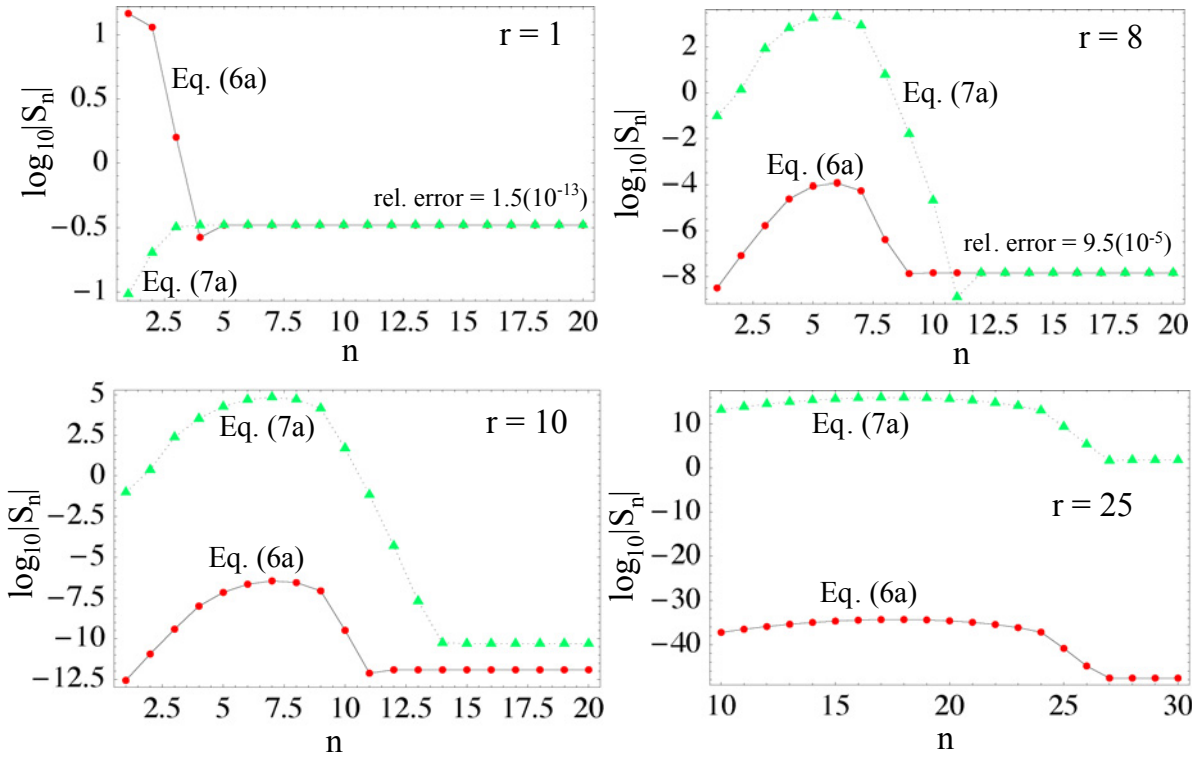

Fig. 4. Partial sums S_n from 0 to n in the evaluation of $Je_{2r}(s,0)$ for $s = 40$, comparing the convergence of Eq. (6a) and Eq. (7a).

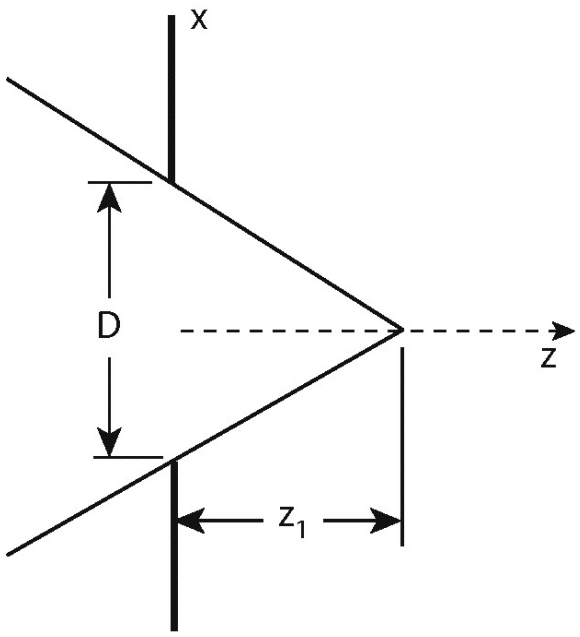

Fig. 5. Converging wave focused at z_1 behind a screen with slot width D.

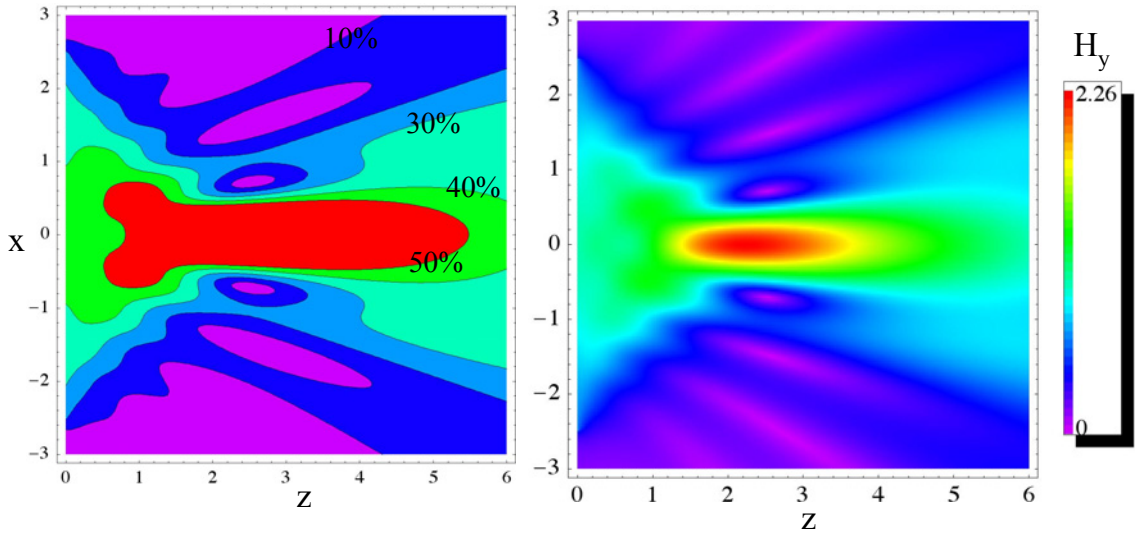

Fig. 6. Contour and density plots of the H_y field behind the slot of width $D = 5\lambda$ for a converging dipole wave with H_y polarization focused at $z_1 = 2.5\lambda$. The results are from a 2D moment method solution.

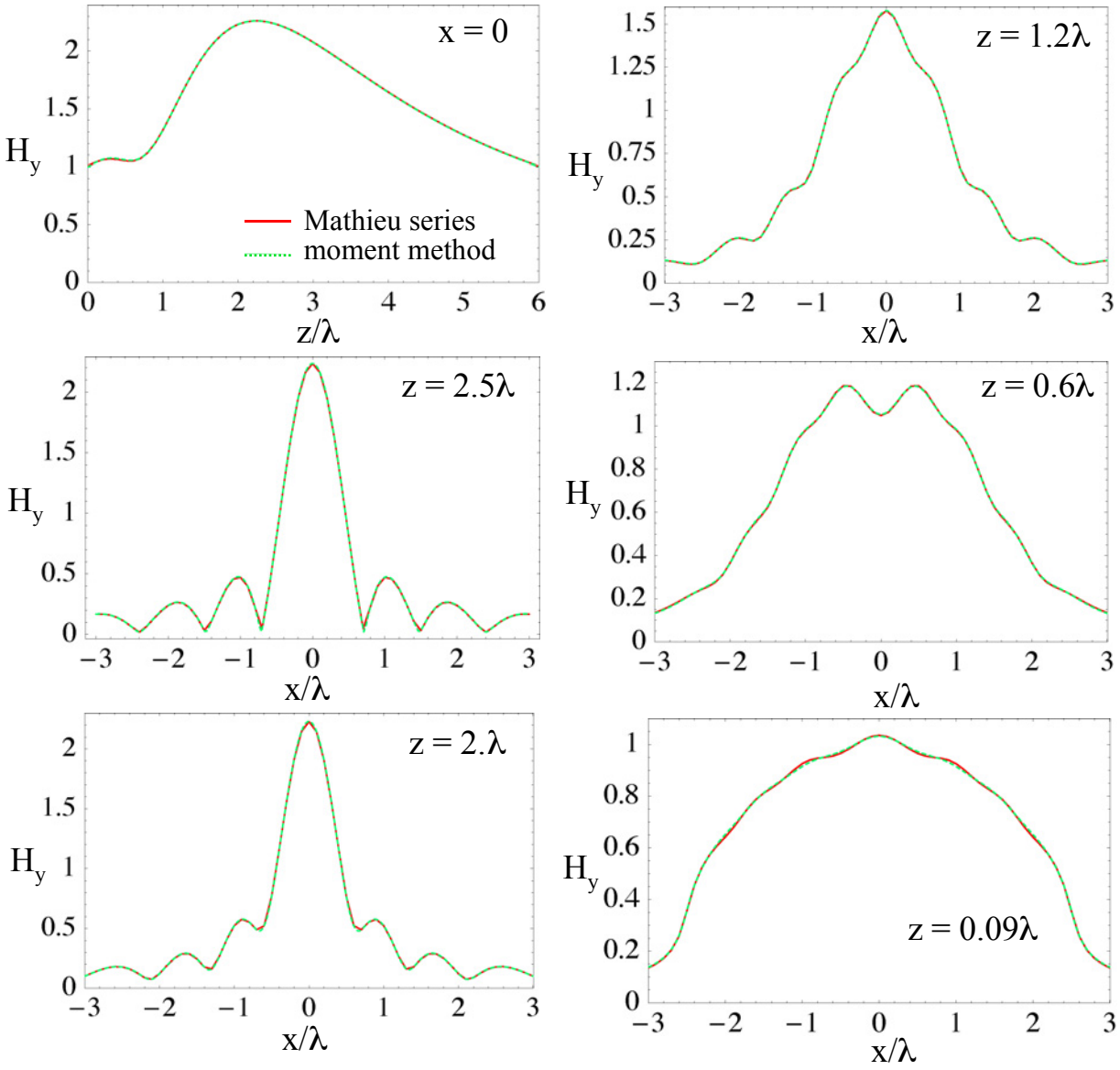

Fig. 7. Field plots for a converging dipole wave with H_y polarization focused at $z_1 = 5\lambda$ behind a slot with width $D = 2.5\lambda$.

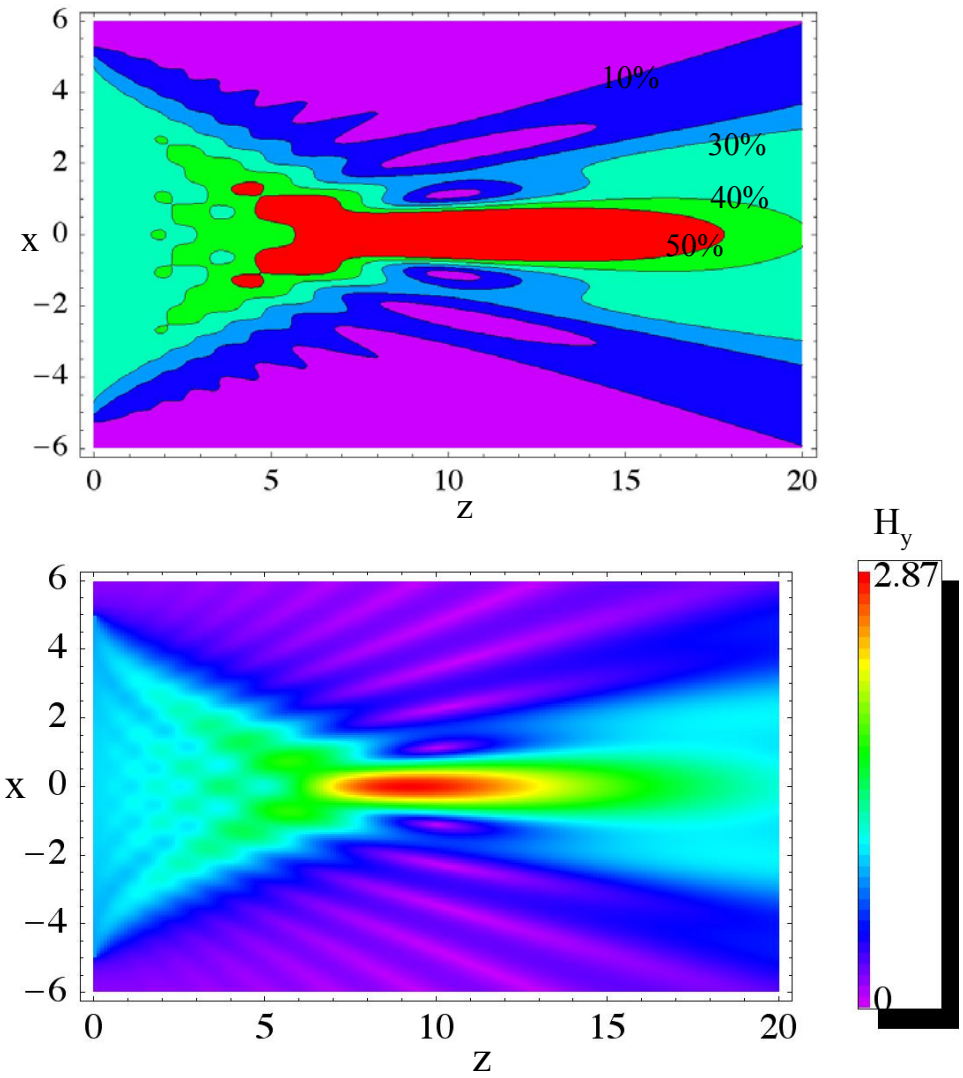

Fig. 8. Contour and density plots of the H_y field behind the slot of width $D = 10\lambda$ for a converging dipole wave with H_y polarization focused at $z_1 = 10\lambda$. The results are from a 2D moment method solution.

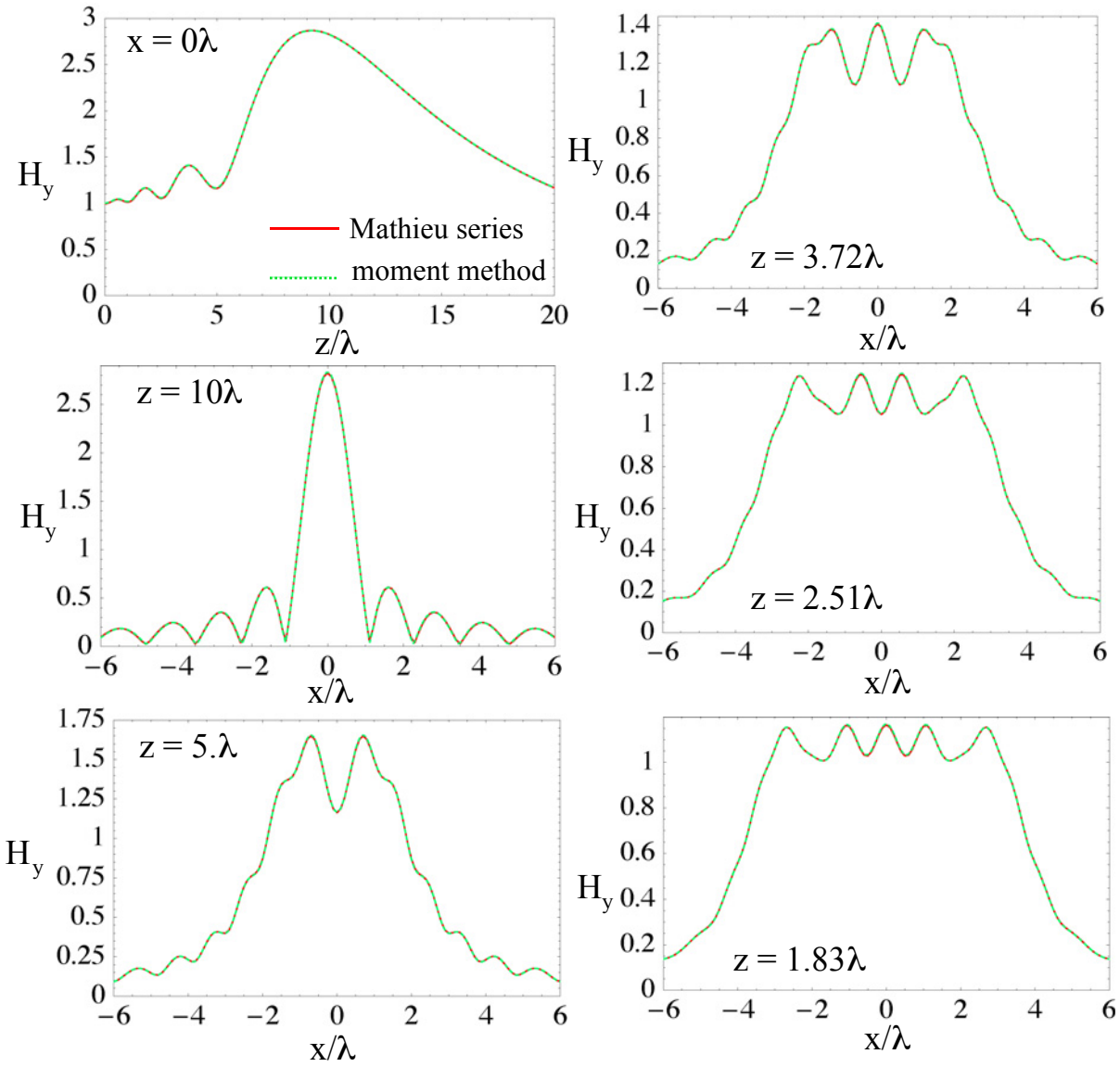

Fig. 9. Field plots for a converging dipole wave with H_y polarization focused at $z_1 = 10\lambda$ behind a slot with width $D = 10\lambda$.

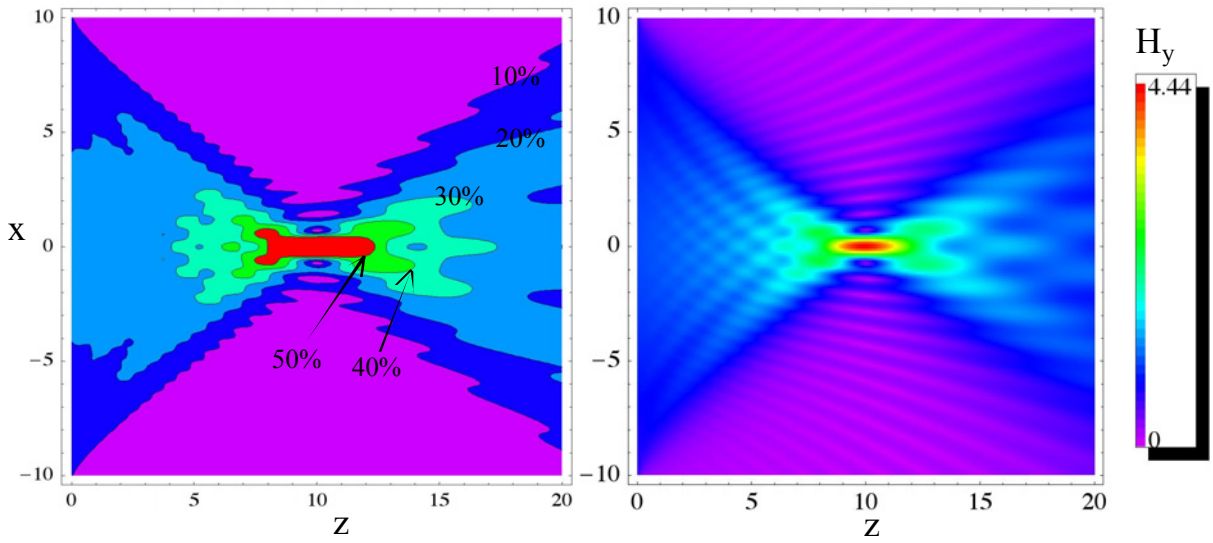

Fig. 10. Contour and density plots of the H_y field behind the slot of width $D = 20\lambda$ for a converging dipole wave with H_y polarization focused at $z_1 = 10\lambda$. The results are from a 2D moment method solution.

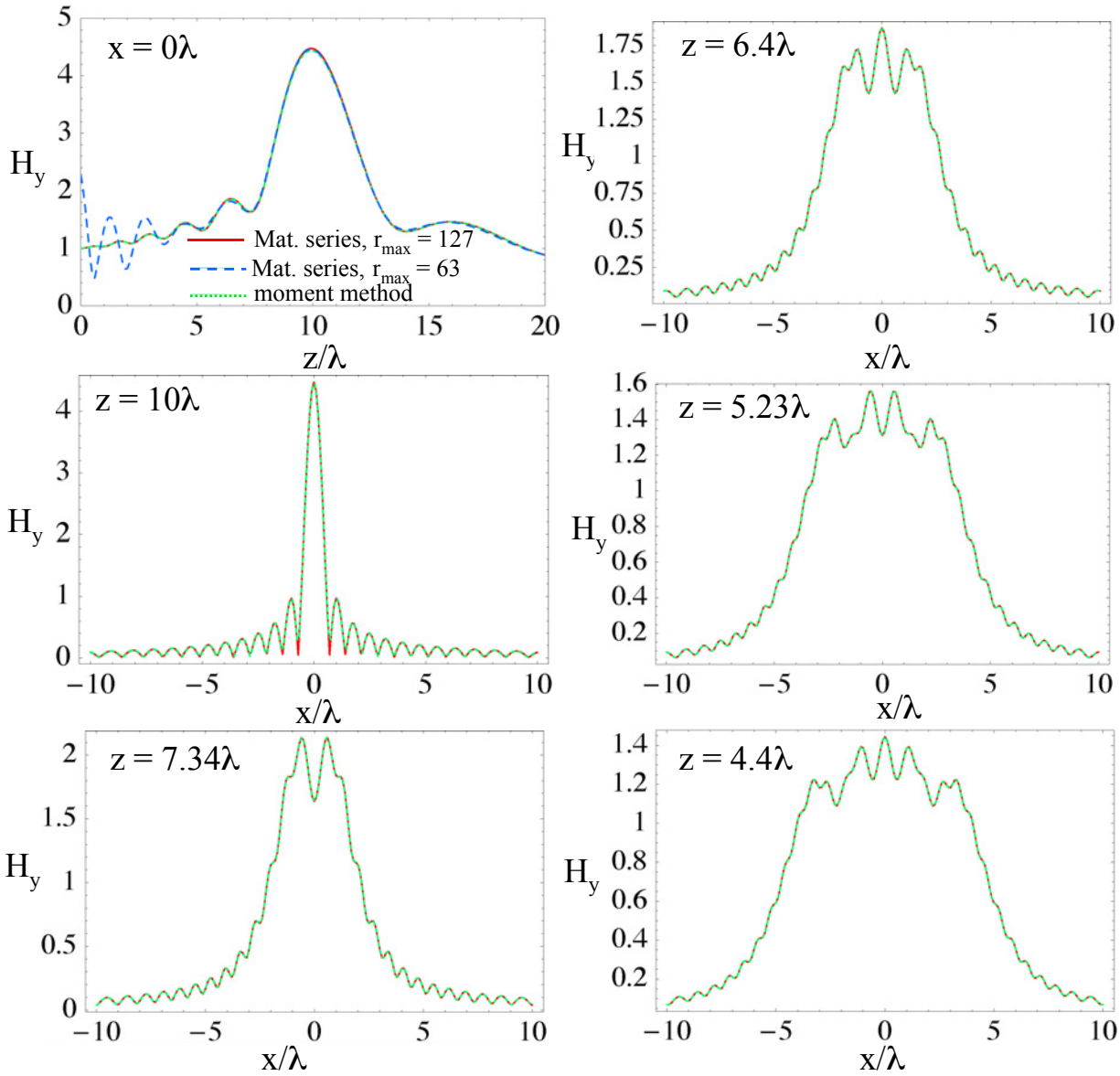

Fig. 11. Field plots for a converging dipole wave with H_y polarization focused at $z_1 = 10\lambda$ behind a slot with width $D = 20\lambda$.

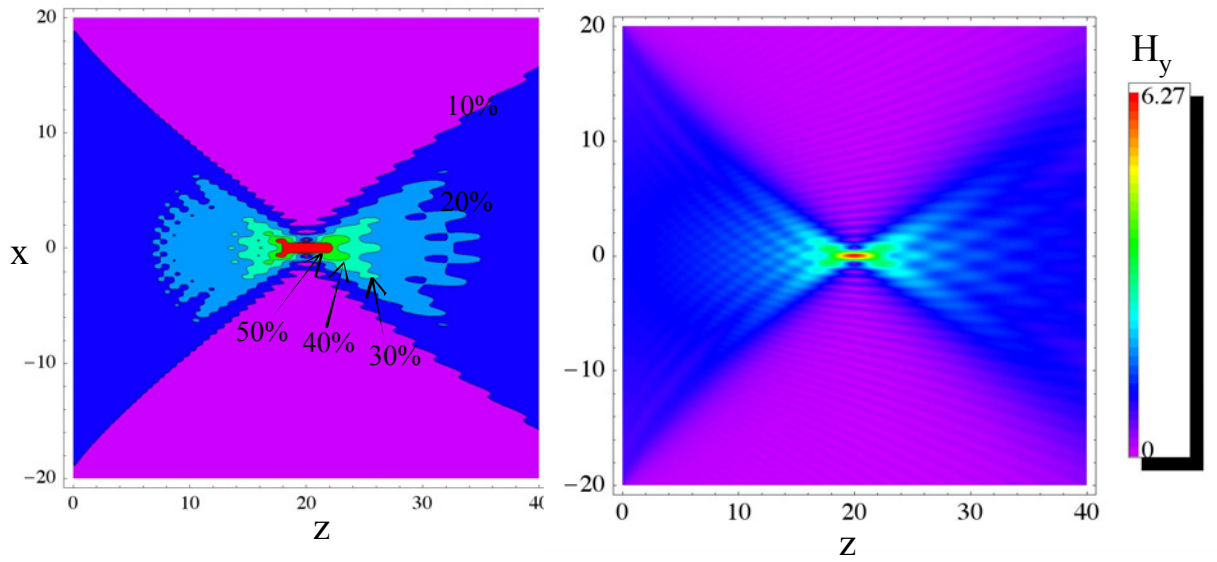

Fig. 12. Contour and density plots of the H_y field behind the slot of width $D = 40\lambda$ for a converging dipole wave with H_y polarization focused at $z_1 = 20\lambda$. The results are from a 2D moment method solution.

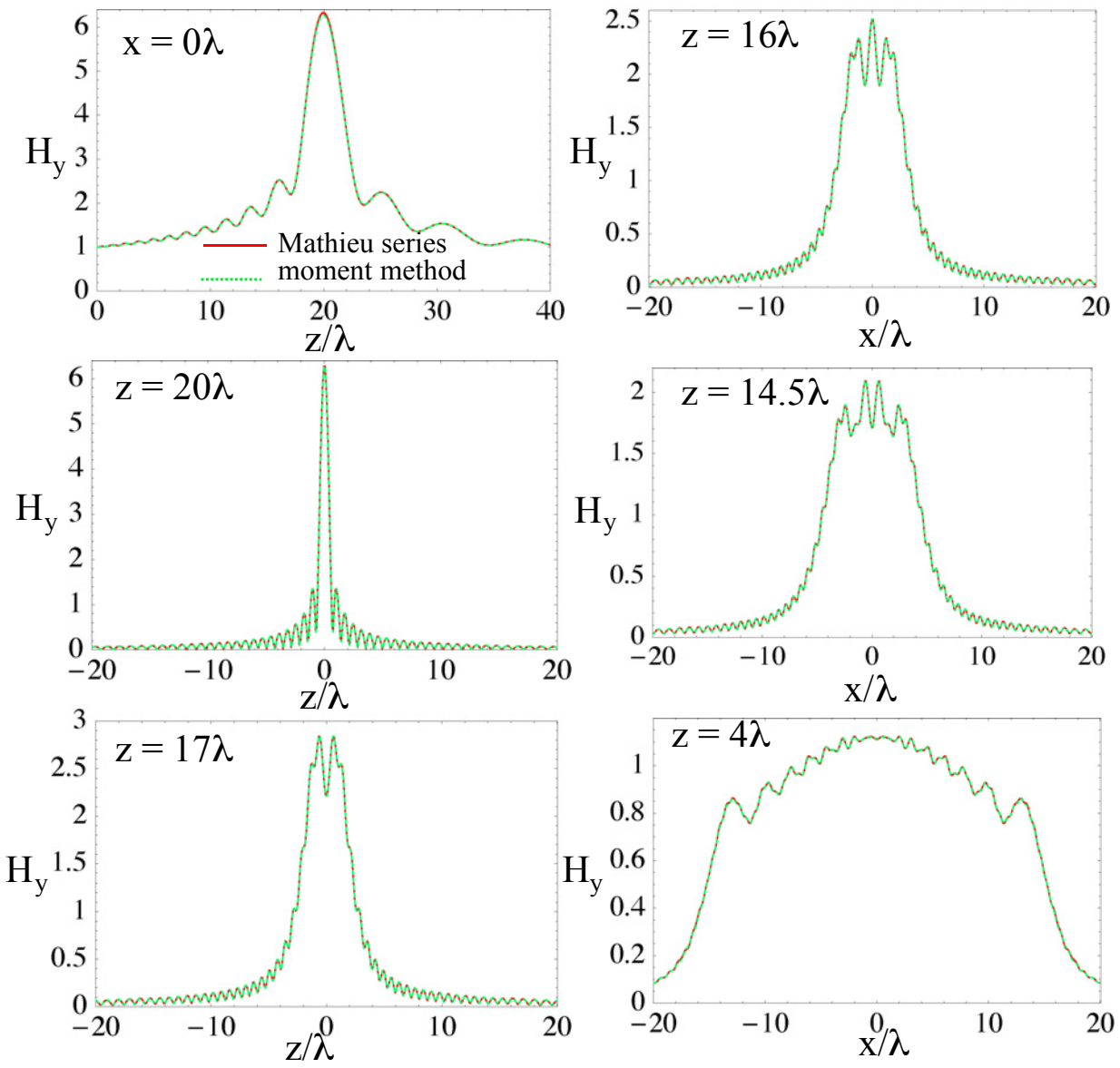

Fig. 13. Field plots for a converging dipole wave with H_y polarization focused at $z_1 = 20\lambda$ behind a slot with width $D = 40\lambda$.

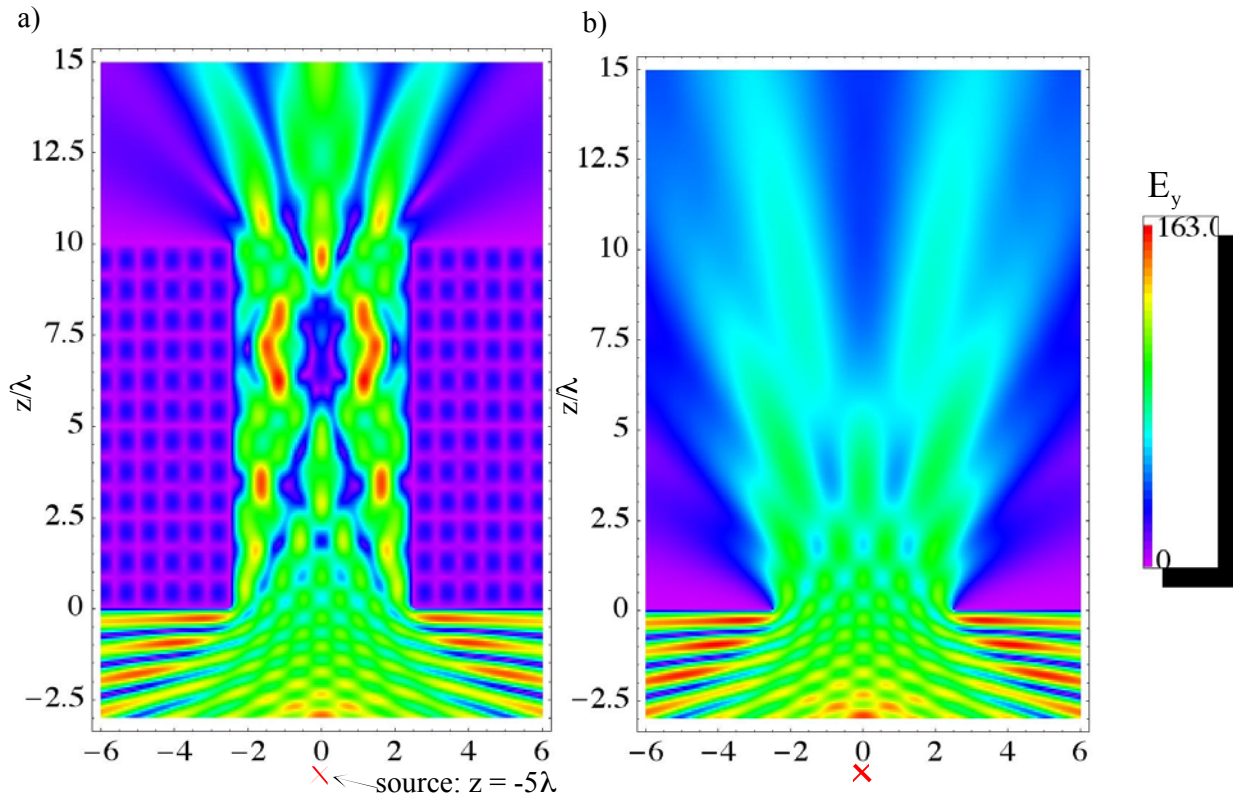

Fig. 14. Electric field E_y due to an electric current line source at $z = -5\lambda$; a) 10λ by 10λ cylinders with 5λ gap, b) screen with 5λ gap.

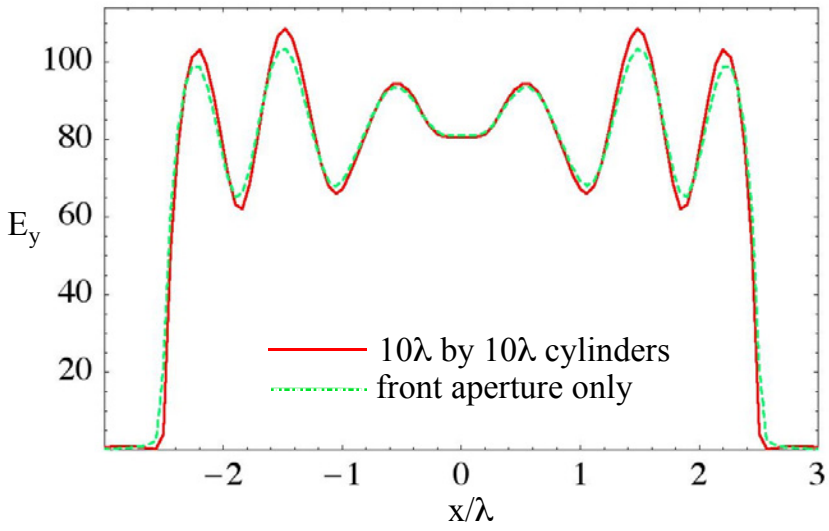

Fig. 15. Electric field E_y due to an electric current line source at $z = -5\lambda$ comparing E_y in the entrance aperture between 10λ by 10λ cylinders with 5λ gap and in a 5λ gap in a thin screen.